Chemical Syntheses of Nanocrystalline Nickel Aluminides

Joel A. Haber,[†] Nilesh V. Gunda,[‡] John J. Balbach,[§] Mark S. Conradi,[§] and William E. Buhro*[,†]

Departments of Chemistry, Physics, and Mechanical Engineering, Washington University, St. Louis, Missouri, 63230-4899

Received August 11, 1999. Revised Manuscript Received February 8, 2000

Nanocrystalline nickel aluminides (nano-NiAl and nano-Ni_3Al) are synthesized by reactions of $NiCl_2$ and $LiAlH_4$ in Et_2O or 1,3,5-trimethylbenzene, followed by annealing of the reaction products at 550−750 °C. The reaction pathways followed in the two solvents differ, leading to nanocrystalline materials of different composition and microstructure. The nanocrystalline nickel aluminide powders are highly susceptible to adventitious oxidation, which produces Al_2O_3. Consolidates obtained by hot pressing the powders at 700−1200 °C and 350−650 MPa in an Ar atmosphere contain 8−23 wt % Al_2O_3. They possess densities of 80−98% of theory, and Vickers microhardnesses of 4.0−6.3 ± 0.3 GPa. Hot-pressing temperatures of ≥ 1200 °C are required to produce consolidates having good environmental stability. Consolidates are also produced by hot pressing admixtures of nano-Ni and nano-Al, with and without added nano-AlN as a second, reinforcement phase. The resulting nanocrystalline and nanocomposite nickel aluminides exhibit the highest purities, densities, and hardnesses (up to 7.4 ± 0.9 GPa) among the samples studied.

Introduction

We previously reported that solvent-based reactions of nickel or titanium chlorides and lithium aluminum hydride ($LiAlH_4$) afforded solids from which nanocrystalline aluminide intermetallics were obtained upon annealing.[1] We now provide complete details of the synthesis and characterization of nanocrystalline NiAl (nano-NiAl) and nanocrystalline Ni_3Al (nano-Ni_3Al) prepared by this method. The syntheses were conducted in both ether and aromatic solvents, and the reaction pathways for each were elucidated. The resulting nanocrystalline powders were consolidated to dense compacts by hot pressing, and the conditions necessary to produce nanocrystalline consolidates with good grain-size and environmental stability were established. The nanocrystalline nickel aluminides produced were susceptible to adventitious oxidation, and the consolidates were found to be nickel aluminide/alumina nanocomposites.

Intermetallic aluminides such as NiAl and Ni_3Al have existing and potential high-temperature structural applications because of their low densities, high melting temperatures, high thermal conductivities, oxidation resistance at elevated temperatures, and high strengths; however, their use is limited by room-temperature brittleness and poor high-temperature creep resistance.[2−4] Refinement of grain sizes to nanometer dimensions has been proposed as a method of inducing room-temperature ductility[5,6] and superplasticity.[7] Indeed, low-temperature superplasticity was recently observed in nanocrystalline Ni_3Al.[8]

Nanocrystalline nickel aluminides have been prepared by a variety of techniques. Most common are gas condensation[9] and mechanical attrition[10] (high-energy ball milling), which produce nanocrystalline powders. Nanometer-scale grain structures have been generated by severe plastic deformation, which may be conducted on massive samples such as ingots, rods, and sheets.[11] Nanocrystalline nickel aluminide powders have also been generated by vapor-phase coreduction of $NiCl_2$ and $AlCl_3$, although single-phase aluminide products were not produced.[12,13] We examined solvent-based chemical synthesis for comparison to the other methods, for its presumed simplicity, and because we expected it to provide good stoichiometric selectivity and control.

In the course of the study, the formation of nanocrystalline nickel aluminides from admixtures of nano-Ni and nano-Al powders was also achieved. To our knowledge, there are few prior reported syntheses of nanocrystalline intermetallics from intimate mixtures of independently prepared nanocrystalline metals.[14−17] Nanocrystalline nickel aluminides and Ni_xAl_y−AlN nanocomposites obtained from these admixtures exhibited the highest purities and hardnesses among the samples studied.

* To whom correspondence should be addressed.E-mail: buhro@wuchem.wustl.edu.
[†] Department of Chemistry.
[‡] Department of Mechanical Engineering.
[§] Department of Physics.

(1) Haber, J. A.; Crane, J. L.; Buhro, W. E.; Frey, C. A.; Sastry, S. M. L.; Balbach, J. J.; Conradi, M. A. *Adv. Mater.* **1996**, *8*, 163−166.
(2) Darolia, R. *JOM* **1991**, *43* (March), 44−49.
(3) Bose, A.; Moore, B.; German, R. M.; Stoloff, N. S. *JOM* **1988**, *40* (September), 14−17.
(4) Jha, S. C.; Ray, R. *JOM* **1990**, *42* (October), 58−61.
(5) Schulson, E. M.; Barker, D. R. *Scripta Metall.* **1983**, *17*, 519−522.
(6) Bohn, R.; Haubold, T.; Birringer, R.; Gleiter, H. *Scripta Metall. Mater.* **1991**, *25*, 811−816.
(7) Alstetter, C. In *Mechanical Properties and Deformation Behavior of Materials Having Ultra-Fine Microstructures*; Nastasi, M., Ed.; Kluwer: Netherlands, 1993; pp 381−399.
(8) McFadden, S. X.; Mishra, R. S.; Valiev, R. Z.; Zhilyaev, A. P.; Mukherjee, A. K. *Nature* **1999**, *398*, 684−686.
(9) Haubold, T.; Bohn, R.; Birringer, R.; Gleiter, H. *Mater. Sci. Eng., A* **1992**, *A153*, 679−683.
(10) Suriñach, S.; Malagelada, J.; Baró, M. D. *Mater. Sci. Eng., A* **1993**, *A168*, 161−164.

10.1021/cm9905186 CCC: $19.00
Published on Web 03/30/2000

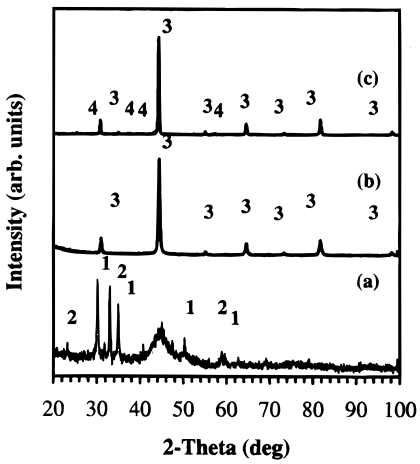

Figure 1. XRD patterns of the products from eq 3. Numeral labels identify the reflections of specific component phases: (a) as-precipitated powder, **1**, LiCl; and **2**, $LiCl{\cdot}H_2O$ (the LiCl hydrate formed from adventitious H_2O exposure during XRD data acquisition); (b) powder annealed at 750 °C in vacuo, **3**, NiAl (30 nm coherence length); (c) sample hot-pressed at 1200 °C, **3**, NiAl (45 nm coherence length); and **4**, Al_2O_3 (60 nm coherence length).

Results

The Ni−Al phase diagram contains five intermetallic compounds: Ni_3Al, Ni_5Al_3, NiAl, Ni_2Al_3, and $NiAl_3$.[21] Two of these five phases, Ni_3Al and NiAl, were the synthetic targets of the present study. Ideally, the specific intermetallic phase produced by reaction of $NiCl_2$ and $LiAlH_4$ would be controlled by the stoichiometry as proposed in eqs 1 and 2. Indeed, reactions conducted in 1,3,5-trimethylbenzene ultimately gave the intermetallics predicted by eqs 1 and 2. However, reactions conducted in Et_2O gave Al-deficient intermetallics and Al_2O_3, necessitating the use of excess $LiAlH_4$ to produce the desired intermetallic phase (eqs 3 and 4). The results established different reaction pathways for syntheses conducted in the two solvents, as described below.

$$4NiCl_2 + 5LiAlH_4 \xrightarrow[164\ °C]{1,3,5\text{-}Me_3C_6H_3} 4NiAl + AlCl_3 + 5LiCl + 10H_2 \quad (1)$$

$$12NiCl_2 + 9LiAlH_4 \xrightarrow[164\ °C]{1,3,5\text{-}Me_3C_6H_3} 4Ni_3Al + 5AlCl_3 + 9LiCl + 18H_2 \quad (2)$$

$$4NiCl_2 + 6.25LiAlH_4 \xrightarrow[Et_2O,\ -20\ °C]{[O]} 4NiAl + 0.84Al_2O_3 + 0.58AlCl_3 + 6.25LiCl + 12.5H_2 \quad (3)$$

$$12NiCl_2 + 11.2LiAlH_4 \xrightarrow[Et_2O,\ -20\ °C]{[O]} 4Ni_3Al + 1.46Al_2O_3 + 4.27AlCl_3 + 11.2LiCl + 22.4H_2 \quad (4)$$

Synthesis of Nickel Aluminides in Et_2O. The syntheses represented in eqs 3 and 4 proceeded rapidly upon addition of Et_2O solutions of $LiAlH_4$ to stirred slurries of $NiCl_2$ at −20 °C. Fine black powders containing amorphous products and crystalline LiCl were produced (Figure 1a).

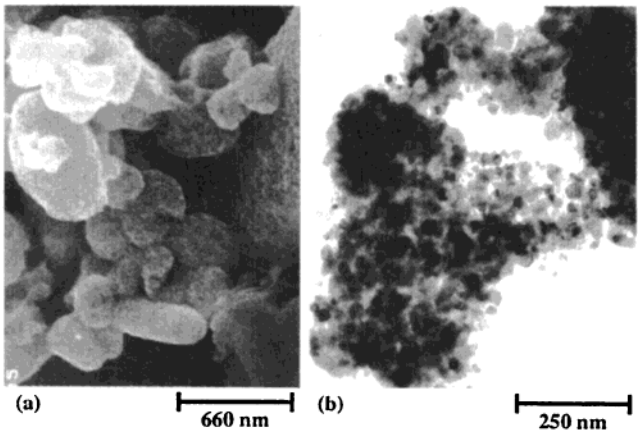

Figure 2. Electron micrographs of an eq 4 Ni_3Al powder annealed at 650 °C in vacuo: (a) SEM image showing that product aggregates have ≤20 nm features; and (b) TEM image showing that aggregates are composed of dark, 10−30 nm Ni_3Al crystallites in a semitransparent (alumina) matrix.

The XRD patterns contained broad features centered on the positions for the strongest reflections of the expected intermetallic phases (Figure 1a), suggesting that amorphous nickel aluminides were primary constituents of the as-precipitated powders. The powders were heated to 650−750 °C under dynamic vacuum (10^{-3} Torr, 10^{-1} Pa) to remove the LiCl byproduct by sublimation and to crystallize the intermetallic phase(s). Mixtures of the desired intermetallic phase and Al-deficient intermetallic phases (by XRD, patterns not shown) were obtained from the reactant stoichiometries given in eqs 1 and 2 when Et_2O was used as the solvent. However, formation of the undesired, Al-deficient intermetallics was avoided by employing $LiAlH_4$ in molar quantities 25% greater than those indicated in eqs 1 and 2. Thus, the powders produced from eqs 3 and 4 in Et_2O and annealed as above gave NiAl and Ni_3Al, respectively, as the only aluminide phases detected by XRD (see Figures 1b and S1).

The additional $LiAlH_4$ was required to replace Al consumed in the formation of Al_2O_3, which was apparently due to oxygen abstraction from Et_2O. That the Al_2O_3 formed prior to or during the 550−750 °C anneal was supported by two observations. First, scanning and transmission electron microscopy (SEM and TEM) of powders annealed at 550−750 °C (Figure 2) revealed 0.2−3.5 μm aggregates of 10−30 nm nickel aluminide crystallites in Al- and O-rich matrices (by EDS). The latter appeared to consist of amorphous or very fine-grained (≤2 nm) Al_2O_3. Electron diffraction patterns (not shown) of the aggregates matched the aluminide phase(s) detected by XRD. Second, the annealed powders were subsequently annealed at a higher temperature, 1100 °C for ≥10 h, or hot-pressed at 1200 °C for 3 h to crystallize the Al_2O_3. Crystalline Al_2O_3 was then detected by XRD (Figure 1c). These observations suggested that Al_2O_3 formed early in the processing, either by decomposition of Et_2O during the solution-phase step, or by decomposition of Et_2O strongly adsorbed to product powders during the initial stages of heat treatment.

The specific reaction stoichiometries proposed in eqs 3 and 4 were based on analyses and assumptions detailed in the section Properties of Consolidated Nickel Aluminide Pellets, below. (Quantitative elemen-

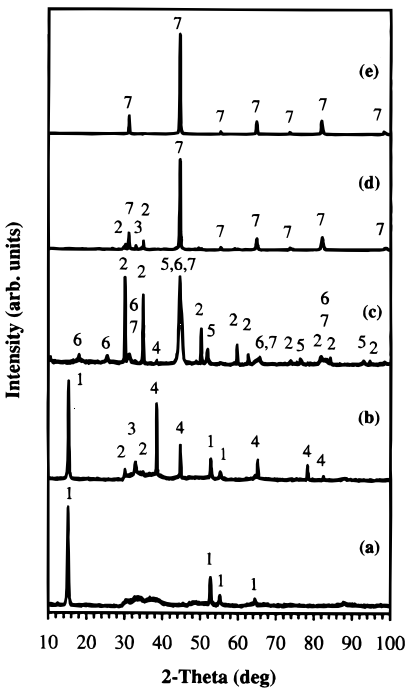

Figure 3. XRD patterns of the products from eq 1 after the powders were annealed at progressively higher temperatures. Numeral labels identify the reflections of specific component phases: (a) the nickel chloride starting material, **1**, $NiCl_2$ (note that peak intensities do not match JCPDS card 1-1134); (b) as-precipitated powder, **1**, $NiCl_2$; **2**, LiCl; **3**, $LiCl·H_2O$; and **4**, Al (∼100 nm coherence length) (the LiCl hydrate formed from adventitious H_2O exposure during XRD data acquisition); (c) powder annealed at 300 °C under N_2, **2**, LiCl; **4**, Al; **5**, Ni (25 nm coherence length); and **6**, intermediate Ni_2Al_3 (15 nm coherence length); (d) powder annealed at 550 °C under N_2, **2**, LiCl; **3**, $LiCl·H_2O$; and **7**, NiAl (28 nm coherence length); and (e) powder annealed at 750 °C in vacuo, **7**, NiAl (47 nm coherence length).

tal analyses, which helped to establish the reaction stoichiometries, were conducted on consolidated pellets.) The $AlCl_3$ byproduct was detected by XRD in related syntheses conducted in 1,2-dimethoxyethane. All products and byproducts were directly observed, except H_2. The results were consistent with the formation of amorphous nickel aluminides and alumina during the solution-phase step or at low annealing temperatures, which crystallized to nanostructured mixtures during subsequent higher temperature anneals.

Synthesis of Nickel Aluminides in 1,3,5-Trimethylbenzene. Reactions conducted in the aromatic solvent according to eqs 1 and 2 at 164 °C ultimately produced the expected intermetallic products without addition of excess $LiAlH_4$. However, the reactions did not directly form the intermetallic phases during the solvent step; rather, the as-precipitated powders from the solvent step required annealing to drive the reactions to completion.

The reaction pathway for eq 1 was examined by XRD analysis of powders annealed at progressively higher temperatures. The as-precipitated powders contained unreacted $NiCl_2$ (Figure 3a), LiCl, and metallic Al (Figure 3b) as crystalline components. The XRD pattern was unchanged after heating the powder to 150 °C. The XRD pattern of powder annealed at 300 °C under N_2 contained no $NiCl_2$ reflections, stronger LiCl reflections than the as-precipitated powder, and reflections for Ni, Al, and Ni_2Al_3 (Figure 3c). Further heating to 550 °C enabled complete reaction to nano-NiAl (Figure 3d), and the LiCl was removed by sublimation at 750 °C in vacuo (Figure 3e). The observed product and intermediate phases had broadened XRD line widths consistent with nanometer-scale crystallite sizes. These results are representative of those found for both eqs 1 and 2; nanocrystalline Al formed during the solvent step, nanocrystalline Ni formed upon annealing, and the expected nickel aluminide product formed in subsequent higher temperature anneals, apparently by reaction of nanocrystalline Al and Ni.

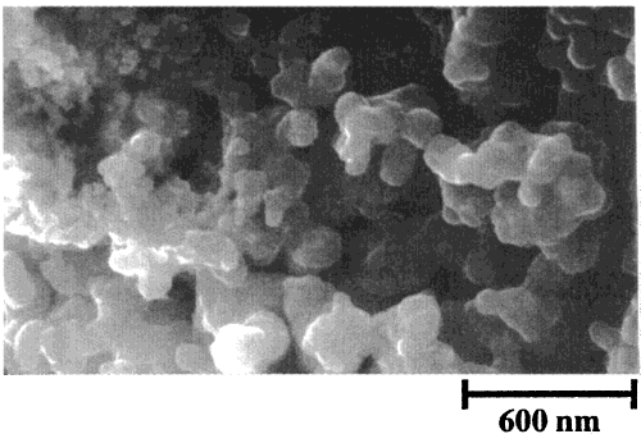

Figure 4. SEM image of NiAl produced by eq 1 and annealed at 650 °C in vacuo; representative of the microstructures of eq 1 and 2 powders in most regions.

In synthetic procedures the as-precipitated powders from eqs 1 and 2 were annealed in a single operation, rather than in the stepwise manner described above. Typically, powders were degassed at ≤150 °C for ≥12 h, and then heated to 550 °C. When the furnace temperature reached 290−350 °C the powders ignited suddenly with an orange flash, and black powder was expelled from the heated portion of the tube with the evolution of a large volume of gas (∼25 mL at STP/g of powder). The gas evolved was determined (by mass spectrometry) to consist primarily of H_2 with small amounts of organic compounds, including CH_4. After removal of the byproduct LiCl by sublimation at 650 °C nano-NiAl (Figure S2a) or nano-Ni_3Al (Figure S2b) were the only crystalline phases detected by XRD.

SEM revealed that the nano-NiAl and nano-Ni_3Al powders consisted of 20−500 nm aggregates of sintered, rounded, 20−50 nm particles (Figure 4). However, some regions of the Ni_3Al powders contained aggregates of cuboidal particles with sharp edges and steps (Figure S3), suggesting that temperatures near or above the melting point of Ni_3Al (1383 °C) had been reached in the exothermic reaction stage. The microstructures in Figure 4 were notably different than those observed for eq 3 and eq 4 powders (Figure 2); they were denser, partially sintered, and missing the diffuse aluminum oxide matrices. These observations and the stoichiometric consumption of $LiAlH_4$ in eqs 1 and 2 suggested that large-scale formation of aluminum oxides had not yet occurred at this stage in the syntheses.

NMR Characterization of the Amorphous Precipitates from Eqs 1 and 2. The progression of crystalline phases along the reaction pathways for eqs 1 and 2 have been detailed above. To assist in identi-

fication of amorphous components, the *as-precipitated* powders from eqs 1 and 2 were further investigated by static (not MAS) solid-state ^{1}H, ^{27}Al, and ^{7}Li NMR. The samples were weakly magnetic (the as-precipitated powders were readily attracted to a hand-held magnet, and affected the lock signal when inserted into the instrument), consequently short T_2*s from FID decays (5−10 μs) were observed for the ^{1}H, ^{7}Li, and ^{27}Al nuclei. Correspondingly, the field inhomogeneities produced broad peaks in the frequency spectra, preventing resolution of different species by chemical shift.

^{1}H spin counts of the as-precipitated powder from eq 1 dried in vacuo at room temperature and 100 °C found 0.44 wt % H and 0.27 wt % H, respectively. The H content determined by NMR was in good agreement with the amount determined by elemental analysis (0.39 and 0.29 wt % for powder dried in vacuo at room temperature and 100 °C, respectively). In the precipitates from eq 2 dried in vacuo at room temperature and 100 °C, NMR found 0.21 wt % H and 0.19 wt % H, respectively. The ^{1}H T_1 relaxation was multiexponential, with ∼30% of the protons relaxing very rapidly and the remainder relaxing much more slowly. Most of the H relaxed with the longer T_1 (∼5−10 s) and thus appeared to be immobile, and not closely associated with the paramagnetic ions, but the nonexponential decay is consistent with relaxation by paramagnetic dopants.[22] The smaller fraction of the H atoms relaxed with a very short T_1 (≤ 5 ms) and thus appeared to be mobile or close to the paramagnetic centers. The sharp break between the rapidly and slowly relaxing components indicated two different chemical environments. Drying the powders in vacuo at 100 °C slightly decreased the total amount of H present and slightly decreased the amount of the rapidly relaxing component relative to the slowly relaxing component. Together the data were consistent with 30% of the H being contained in residual organic molecules (likely adsorbed solvent) and with 70% being contained in LiH.

All of the signal detected by ^{27}Al NMR was consistent with Al in the metallic state. The short T_1 (6.4 ms) was also consistent with relaxation by the Korringa mechanism,[23] as in pure Al metal. The Al peak was shifted 1600 ppm to higher frequency from the $AlCl_3$ (aq) reference, the characteristic frequency (Knight) shift[23] from conduction electrons in Al metal. No signal from $AlCl_3$ or other nonmetallic Al compounds was detected; an $AlCl_3$ sample was examined for comparison. Thus, $AlCl_3$ was not produced during the solvent step with this solvent, unlike the syntheses conducted in Et_2O (eqs 3 and 4).

No metallic Li was detected by ^{7}Li NMR. The nonexponential T_1 (∼50 s) was much longer than that of metallic Li (∼150 ms), consistent with static, nonmetallic Li relaxed by paramagnetic impurities.[22] Further, as a sensitive (negative) test for a small fraction of ^{7}Li in metallic species with short relaxation times, no change in peak shift was observed with different recovery times. The elemental analysis, solid-state NMR, and quantity of gas evolved during the SHS reaction were all consistent with a H:Li ratio of ∼50% in the precipitated powder (i.e., there were similar amounts of LiCl and LiH). Thus, the as-precipitated powder likely consisted of an intimate mixture of $NiCl_2$, $NiCl_x$ ($x < 2$), nano-Al, LiH, and LiCl, with LiH and nano-Al acting as reducing agents for the nickel chlorides during the subsequent solid-state reaction.

Synthesis of Nickel Aluminides from Admixtures of Nano-Ni and Nano-Al. Elucidation of the reaction pathway for eqs 1 and 2 indicated that Al and Ni were first formed as separate phases, which subsequently reacted to afford nickel aluminides. This finding suggested that annealing admixtures of separately prepared nano-Al and nano-Ni powders should also afford nanocrystalline nickel aluminides. Such an approach was undertaken, in some cases with nano-AlN added as a reinforcement phase.

Chemical syntheses of nano-Al, nano-Ni, and nano-AlN were developed to produce the constituent phases for subsequent reaction. The nano-Al was produced by thermal decomposition of $H_3Al(NMe_2Et)$, as described elsewhere,[18] and had a mean crystallite diameter of 50−130 nm. The nanowhisker-rich nano-AlN, produced as described elsewhere,[19,20] contained ∼50% nanowhiskers, which were between 20 and 100 nm in diameter with aspect ratios of 20−100. Nanocrystalline Ni was synthesized by reduction of $NiCl_2$ with $LiBEt_3H$ in refluxing 1,3,5-trimethylbenzene, and purified by washing with MeOH and H_2O to remove LiCl (see the Experimental Section). The nano-Ni so obtained was free of other crystalline or nanocrystalline phases by XRD (Figure S4). TEM images (Figure S5) revealed 20−300 nm agglomerates of 2−10 nm Ni particles. Residual Cl (0−1.8 atom %) was detected in the Ni aggregates by EDS.

The separate nanocrystalline phases were admixed by ultrasonic cosuspension in a dispersing liquid. The liquid was removed in vacuo while sonication continued, ultimately affording dry powders. TEM images and EDS of powders co-suspended in hexane indicated that nano-Al and nano-Ni were well intermixed in this liquid, but that the nano-AlN was poorly suspended and not well mixed with the nano-Ni and nano-Al. Indeed, the resulting pellets consolidated from such admixtures (see below) were poorly densified and contained 10−20 μm and ≥150 μm regions of segregated nano-AlN particles. In contrast, TEM images and EDS of powders cosuspended in pyridine (Figure S6) indicated that the AlN was well suspended and intimately mixed with the nano-Ni and nano-Al. The resultant pellets were denser,

(11) Valiev, R. Z.; Korznikov, A. V.; Mulyukov, R. R. *Mater. Sci. Eng., A* **1993**, *A168*, 141−148.
(12) Sohn, H. Y.; PalDey, S. *J. Mater. Res.* **1998**, *13*, 3060−3069.
(13) Sohn, H. Y.; PalDey, S. *Metall. Mater. Trans. B* **1998**, *29B*, 465−469.
(14) Dickenscheid, W.; Birringer, R. *J. Appl. Phys.* **1995**, *77*, 533−539
(15) Mori, H.; Yasuda, H. *J. Microscopy* **1995**, *180*, 33−38.
(16) Liu, Z. G.; Guo, J. T.; He, L. L.; Hu, Z. Q. *Nanostruct. Mater.* **1994**, *4*, 787−794.
(17) Gryaznov, V. G.; Trusov, L. I. *Prog. Mater. Sci.* **1993**, *37*, 289−401.
(18) Haber, J. A.; Buhro, W. E. *J. Am. Chem. Soc.* **1998**, *120*, 10847−10855.
(19) Haber, J. A.; Gibbons, P. C.; Buhro, W. E. *J. Am. Chem. Soc.* **1997**, *119*, 5455−5456.
(20) Haber, J. A.; Gibbons, P. C.; Buhro, W. E. *Chem. Mater.* **1998**, *10*, 4062−4071.
(21) *Binary Alloy Phase Diagrams*; Massalski, T. B., Ed.; American Society for Metals: Metals Park, OH, 1986; pp 142−143.
(22) Abragram, A. *Principles of Nuclear Magnetism*; Clarendon: Oxford, 1994; pp 378−389.
(23) Slichter, C. P. *Principles of Magnetic Resonance*; Springer: New York, 1996; pp 113−127 and 156.

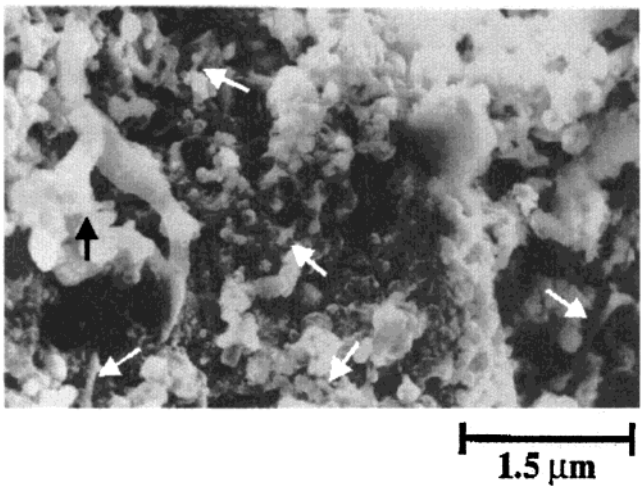

Figure 5. SEM image revealing well-dispersed nano-AlN whiskers (identified by arrows) in a fracture surface of pellet fragment obtained by annealing a nano-Al, nano-Ni, and nano-AlN powder admixture at 400 °C in vacuo.

and SEM images of the pellets did not show regions of segregated nano-AlN particles.

A powder admixture of nano-Ni, nano-Al, and nano-AlN was pressed into a pellet at 150 °C and then placed in a quartz tube under a dynamic vacuum. The encapsulated sample was heated in a tube furnace to effect reaction of the nano-Ni and nano-Al phases, which were present in relative amounts consistent with formation of nano-NiAl. The furnace was gradually heated to 400 °C, at which temperature an ignition event was indicated by the deposition of a black film on the cool portion of the tube outside the furnace and by expulsion of pellet fragments from the hot zone. The evolution of phases in this sample is charted in Figure S7. The pellet fragments produced XRD reflections for nano-NiAl and nano-AlN, and no reflections for residual Al or Ni (Figure S7). Minor reflections for Ni_3Al indicated that the product was slightly Al deficient, although the reactant mixture had been slightly Al rich. Thus, temperatures sufficiently high to vaporize Al in vacuo had likely been achieved, which suggested that the black film deposited was metallic Al. SEM micrographs (Figures 5 and S8) confirmed the retention of nanometer grain sizes and showed well-dispersed AlN nanowhiskers in the pellet fragments.

To prevent fragmentation and Al loss and to achieve full density, all subsequent pellets were reacted in a hot press under a load of 350 MPa at temperatures of up to 1200 °C. XRD analyses confirmed formation of nanocrystalline nickel aluminide phases in the hot-pressed pellets. Precursor powder admixtures with NiAl compositions reacted completely, and exhibited no detectable reflections for Ni_3Al. However, precursor powder admixtures with Ni_3Al compositions did not react completely in every case. This may be due to the lower heat of formation of Ni_3Al relative to that for NiAl (−9.4 kcal/g atom or −39 kJ/g atom vs −14.1 kcal/g atom or −59 kJ/g atom, respectively).[24]

SEM images of fracture surfaces of the hot-pressed pellets confirmed the retention of nanometer-sized grains in most areas. However, an Ni_3Al (93 wt %)/AlN (7 wt %) pellet contained regions of larger, 1−8 μm faceted grains (Figure S9), indicating that in some local areas temperatures close to the melting point of Ni_3Al (1380 °C) were reached during the hot-pressing synthetic procedure.

Properties of Consolidated Nickel Aluminide Pellets. Consolidated pellets were also obtained by hot pressing the powders prepared by eqs 1−4. This section gives further characterization and property determination for the nickel−aluminide consolidates produced by the various synthetic methods. Specifically, stability, purity and O content, long-range structural order, and Vickers microhardness of consolidates were assessed.

Hot-pressing temperatures of ≥1200 °C were required to produce pellets with long-term (atmospheric) stability from powders generated by eqs 1−4. Several batches of NiAl (from eqs 1 and 3) and Ni_3Al (from eqs 2 and 4) were consolidated into 13 mm diameter pellets at 700−1200 °C and 350−650 MPa. A NiAl pellet pressed at 700 °C for 1.5 h remained powdery. The pellets pressed at 900−1000 °C initially appeared dense and tough, but upon air exposure crumbled into powder within 2 days to 7 weeks. Pellets pressed at 1200 °C were relatively air stable; a NiAl (eq 1) pellet was air exposed for 1 year with no visible degradation. A Ni_3Al (eq 4) pellet hot pressed at 1000 °C and then sintered at 1300 °C was intact after 1 year of air exposure but was becoming powdery on the edges. Nickel aluminides are susceptible to reaction with oxygen or moisture via grain boundaries, a phenomenon known as pesting, by which consolidates degrade to fine powders without appreciable bulk oxidation. For NiAl, pesting normally occurs at 700−900 °C.[25,26] Because of their high volume fraction of grain boundaries nanocrystalline materials may be especially susceptible to pesting.

The greater stability of the pellets pressed or sintered at ≥1200 °C likely resulted from sintering of the Al_2O_3 contained within the material. The transition aluminas (γ-, δ-, and θ-Al_2O_3) transform without grain growth until the transformation to α-Al_2O_3 at ≥1200 °C, which occurs with rapid grain growth.[27] As discussed below, *all* the consolidates of powders prepared by eqs 1−4 contained oxygen (albeit likely from different sources), and hence Al_2O_3. The pellets consolidated at ≤1000 °C likely contained porous or poorly bonded Al_2O_3, which allowed ready oxygen diffusion into the interior of the consolidate, and consequently degradation by pesting. The pellets pressed or sintered above the transition temperature to α-Al_2O_3 likely contained sintered Al_2O_3, which likely formed a dense protective coating for the nickel aluminide grains.

The consolidates of powders prepared by eqs 1−4 were characterized by XRD, SEM, TEM, and electron microprobe. The phases present and their XRD coherence lengths are given in Table 1. SEM and TEM confirmed that nanometer crystallite sizes were retained during hot pressing (Figure S10), while SEM and microprobe

(24) Kubaschewski, O.; Heymer, G. *Trans. Faraday Soc.* **1960**, *56*, 473−478.

(25) Aitken, E. A. In *Intermetallic Compounds*; Westbrook, J. H., Ed.; John Wiley & Sons: New York, 1967; pp 491−516.

(26) Meier, G. H.; Pettit, F. S. *Mater. Sci. Eng., A* **1992**, *153*, 548−560.

(27) Brinker, C. J.; Scherer, G. W. *Sol-Gel Science*: *The Physics and Chemistry of Sol-Gel Processing*; Academic Press: New York, 1990; pp 599−607.

Table 1. Properties of Consolidates Pressed from Powders Generated by Eqs 1−4

nominal pellet composition (powder source)	phase present (coherence length, nm)	consolidation conditions			density, g/cm^3 (% theor. density)[a]	atmospheric stability	Vickers hardness, GPa	elements detected by EDS (trace elements)	composition,[b] wt %				Al_2O_3	
		T, °C	t, h	P, MPa					Ni	Al	Cl	O	wt %[c]	theor. wt %[d]
NiAl (eq 1)	NiAl (45)	900	3	350		crumbled in < 2 months		Ni, Al, O, (C, S)						
Ni_3Al (eq 2)	Ni_3Al (20), NiAl (minor)	900	3	350	5.1[f] (80)			Ni, Al, O, Cl, (C)	68	15	1	16	11	8
sintered[e]		1300	2	18		edges crumbling after 1 year	4.0 ± 0.2							
NiAl[g] (eq 1)	NiAl (35), Al_2O_3 (45)[h]	1200	2	420	5.5[f] (98)	stored under N_2	5.3 ± 0.3	Ni, Al, O (Cl, C, S, Si)						13
NiAl (eq 3)	NiAl (45), Al_2O_3 (55)[h]	1200	3	350	4.6[f] (87)	air stable for > 1 year	5.9 ± 0.3	Ni, Al, O	53	37	0.3	10	23	20
NiAl (eq 3)	NiAl (40), Al_2O_3 (50)[h]	1200	3	350	5.1[i] (94)		6.3 ± 0.3	Ni, Al, O, (C, S, Si)	56	36	0.3	8	19	20
Ni_3Al (eq 4)	Ni_3Al (30)[h]	1000	3	350	4.8[f] (90)	crumbled within 3 days		Ni, Al, O, (C)	63	18	0.4	19	19	16

[a] The value for theoretical density used in the calculation was the weighted average of the nickel aluminide phase and alumina present; % theor. density is the measured density divided by the theoretical density. [b] Determined by electron microprobe. [c] Calculated from the microprobe data as described in the text in the "Properties of Consolidated Nickel Aluminide Pellets" section. [d] Calculated from the reaction stoichiometry as described in the text in the "Properties of Consolidated Nickel Aluminide Pellets" section. [e] The sample was sintered after XRD and microprobe analyses. [f] Density was determined geometrically. [g] From powder prepared by eq 1, but using a 10% excess of $LiAlH_4$. The powder contained a small amount of Ni_2Al_3 (by XRD); however, after consolidation only NiAl and Al_2O_3 (and graphite) reflections were detected. [h] Minor graphite reflections due to surface contamination by the graphite sleeve used in the hot press were also detected. [i] Density was determined by the Archimedes method.

Figure 6. SEM images of polished nickel aluminide pellets hot pressed at 1200 °C: (a) a Ni_3Al pellet consolidated from eq 2 powder and (b) a NiAl pellet consolidated from eq 3 powder. The diagonal lines evident are polishing scratches. Note the smaller fraction of O-rich dark regions in the eq 2 pellet (a) as compared to the eq 3 pellet (b).

analysis also found compositional heterogeneities on the micrometer length scale (Figure 6). Microprobe area scans analyzing for Ni, Al, and Cl showed that the Cl concentrations were 0.1−1 wt %, and were higher in the light areas (Figure 6). Note the residual Cl levels for these samples were below the level of detection by EDS, indicating the higher sensitivity of the electron-microprobe analyses. Al concentrations were higher in the dark areas than in the light areas, and Ni concentrations were higher in the light areas than in the dark areas. The amount of O was 30−100% greater in the dark areas. EDS established that the dark areas also often contained C, S, and Si impurities. We concluded that the light regions consisted primarily of nickel aluminide phases, and the dark regions primarily of alumina.

The oxygen and Al_2O_3 content of the pellets was estimated in three ways, which produced values in reasonable agreement with one another under the assumption that all O was present as Al_2O_3. First, the weight % of O was estimated by summing the micro-

Table 2. Properties of Consolidates Pressed from Admixtures of Nanocrystalline Starting Phases

nominal pellet composition	quantities of reactant phases used, g (mmol)			phases detected by XRD	density		Vickers hardness (GPa)
	nano-Ni	nano-Al	nano-AlN		g/cm^3	% theor.[a]	
NiAl (72 wt %)/AlN (28 wt %)[b]	1.11 (18.9)	0.533 (19.8)	0.633 (15.4)	NiAl, AlN, Ni_3Al	3.1[c]	67	1.9 ± 0.8
Ni_3Al (89 wt %)/AlN (11 wt %)[b]	2.19 (37.3)	0.313 (11.6)	0.308 (7.52)	Ni_3Al, AlN, NiAl, Ni	5.2[c]	91	5.1 ± 0.6
NiAl (84 wt %)/AlN (16 wt %)[d]	1.21 (20.6)	0.565 (20.9)	0.332 (8.10)	NiAl, AlN	4.2[c]	104	7.4 ± 0.8
NiAl[d]	1.42 (24.2)	0.654 (24.2)		NiAl, impurities	5.36[e]	90	6.6 ± 0.8
Ni_3Al (89 wt %)/AlN (11 wt %)[d]	2.17 (37.2)	0.347 (12.9)	0.322 (7.86)	Ni_3Al, AlN	5.38[e,f]	80	7.4 ± 0.9
Ni_3Al[d]	2.04 (34.8)	0.320 (11.9)		Ni_3Al, Ni, Mo_2C, impurities	6.28[e]	84	6.2 ± 1.2

[a] The value for theoretical density used in the calculation was the weighted average of the phases listed in the nominal pellet composition; % theor. density is the measured density divided by the theoretical density. [b] The mixed powders were cosuspended in hexane for 1.5 h and the pellet pressed for 0.75−1.0 h at 1000 °C under a load of 350 MPa. [c] Density was determined geometrically. [d] The mixed powders were cosuspended in hexane for 3.5 h, resuspended in pyridine for 2 h, and the pellet pressed for 3 h at 1200 °C under a load of 350 MPa. [e] Density was determined by the Archimedes method. [f] The pellet contained a nondensified inclusion due to and near a break in the graphite sleeve used in the hot press.

probe-determined weight percentages of Ni, Al, and Cl, and by assuming the remainder to be O (see Table 1). This overestimates the O content, because other elements such as C, N, and S also contribute to the remainder. Second, the amount of Al determined by microprobe to be present in excess of the stoichiometric amount required for the nickel aluminide phase (by comparison to the amount of Ni) was assumed to be present as Al_2O_3, allowing calculation of an "experimental" Al_2O_3 weight % (see Table 1). Third, a "theoretical" weight % of Al_2O_3 based upon the reactant stoichiometry was calculated by assuming (1) that all of the Li formed LiCl, (2) that any remaining Cl formed $AlCl_3$, (3) that stoichiometric NiAl or Ni_3Al was produced, and (4) that all excess Al produced Al_2O_3 (see Table 1). These estimations indicated that the pellets contained 8−19 wt % O and 8−23 wt % Al_2O_3, which were significant amounts.

Thus, the pellets hot pressed from powders generated by each of eqs 1−4 had high oxygen contents. We previously discussed the origin of O (Al_2O_3) contamination of the powders generated from eqs 3 and 4, which was degradation of the Et_2O solvent. However, the powders generated from eqs 1 and 2, prepared in the nonoxygenated 1,3,5-trimethylbenzene solvent, appeared to be free of extensive oxide contamination immediately after synthesis (see above). We surmised that the high oxide content in pellets pressed from these powders was due to adventitious oxidation during powder storage, handling, and consolidation. Care was taken to maintain inert atmospheres during synthetic operations and powder transfers. Indeed, the hot press was constructed inside an Ar-filled glovebox to protect the powders during die loading and consolidation. However, as we have previously reported nanocrystalline Al powders are exceptionally oxophilic,[18] and react with O_2 at partial pressures of $\geq 10^{-41}$ Torr ($\geq 10^{-39}$ Pa),[28] which are below the levels experimentally achievable by our standard, "inert-atmosphere" techniques. We presume that nanocrystalline nickel aluminide powders are similarly oxophilic. Consequently, all pellets pressed from powders prepared by eqs 1−4 were in fact nickel aluminide/alumina composites. The chemical synthesis of oxide-free nickel aluminide *powders* may not be a practicably obtainable result.

The pellets produced by hot pressing admixtures of nano-Ni and nano-Al (with and without added nano-AlN) were not visually degraded by several weeks of atmospheric exposure, and appeared to be purer (by EDS) than were the pellets hot pressed from powders generated by eqs 1−4. Lower concentrations of O (<5 wt %, likely arising from surface oxidation) and C (likely arising from the surface layer of Mo_2C produced by reaction of the TZM punch with the graphite sleeve) were detected. However, the pellets produced from the nanophase admixtures did contain 0.5−1.5 wt % of Cl distributed relatively uniformly, with some 20 μm regions containing 20−50 wt % Cl (likely unreacted $NiCl_2$ particles). Some areas containing small amounts of Si and S were also detected.

The Vickers microhardnesses of all pellets, regardless of origin, scaled primarily with density and secondarily with reinforcement (Al_2O_3 or AlN) content as indicated in Tables 1 and 2. Dense consolidates were harder than incompletely densified consolidates, regardless of composition. The dense nano-AlN composites were harder than all the other samples. All of the samples were harder than coarse-grained NiAl (2.9−4.9 GPa)[29,30] or Ni_3Al (2.5−4.4 GPa).[31,32] The Vickers microhardness values determined here were within the hardness range previously reported for nano-NiAl (4.5−7.9 GPa)[29,30,33] and nano-Ni_3Al (4.7−8.1 GPa).[31,32] No cracks were observed to extend from the test indentations, suggesting that all of the syntheses produced materials with good fracture toughness.

Discussion

The various reaction pathways for the nickel aluminide syntheses are summarized in Figure 7. This schematic is intended to highlight the similarities and differences between methods, and is not a precise representation of all reaction steps, constituent phases, and microstructures. Reactions of $NiCl_2$ and $LiAlH_4$ conducted in Et_2O (eqs 3 and 4) form amorphous Ni_x-

(28) Fujii, H.; Nakae, H.; Okada, K. *Acta Metall. Mater.* **1993**, *41*, 2963−2971.

(29) Börner, I.; Eckert, J. *Mater. Sci. Forum* **1996**, *225-227*, 377−382.

(30) Smith, T. R.; Vecchio, K. S. *Nanostruct. Mater.* **1995**, *5*, 11−23.

(31) Jang, J. S. C.; Koch, C. C. *J. Mater. Res.* **1990**, *5*, 498−510.

(32) Languillaume, J.; Chmelik, F.; Kapelski, G.; Bordeaux, F.; Nazarov, A. A.; Canova, G.; Esling, C.; Valiev, R. Z.; Baudelet, B. *Acta Metall. Mater.* **1993**, *4*, 2953−2962.

(33) Pyo, S. G.; Kim, N. J.; Nash, P. *Mater. Sci. Eng., A* **1994**, *181/182*, 1169−1173.

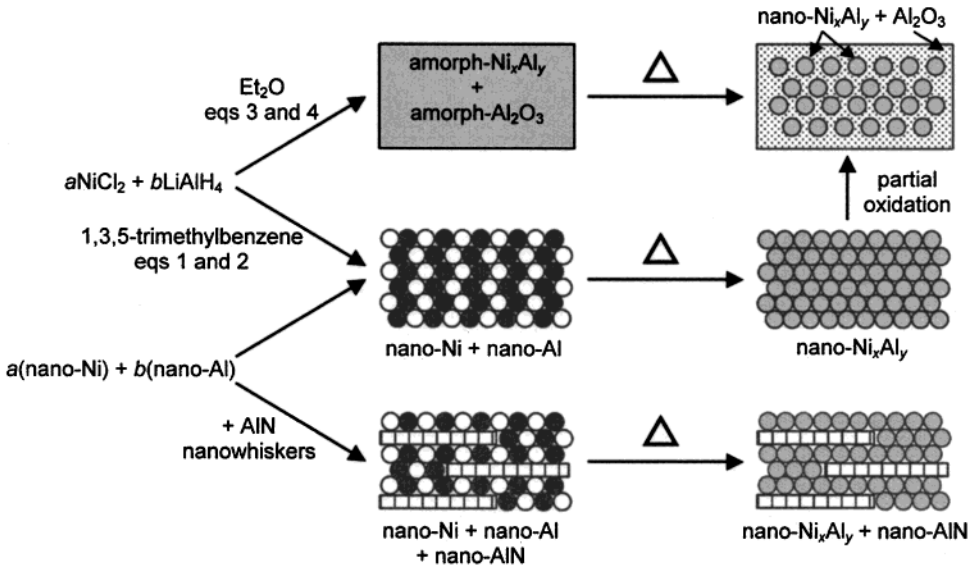

Figure 7. The synthetic results are summarized in this simplified schematic representation of the reaction pathways elucidated. Some intermediates and byproducts are omitted, as are specific annealing and consolidation steps. The microstructural sketches are general, and do not precisely depict specific cases.

Al_y directly from solution, but also form Al_2O_3 in sacrificial side reactions. In contrast, reactions of $NiCl_2$ and $LiAlH_4$ conducted in 1,3,5-trimethylbenzene (eqs 1 and 2) initially form Ni and Al as separate phases, which subsequently react to give Ni_xAl_y upon annealing. The pathway for eqs 1 and 2 is mimicked by reactions among intermixtures of separately prepared nano-Ni and nano-Al phases.

The reaction pathways followed by eqs 1−4 appear to be determined primarily by reactant solubilities. $LiAlH_4$ is a soluble, strong reducing agent in Et_2O,[34] in which $NiCl_2$ is partially cosoluble. Consequently reactions between $LiAlH_4$ and $NiCl_2$ in Et_2O proceed rapidly and completely at −20 °C to produce amorphous nickel aluminides, which crystallize upon annealing. In contrast, $LiAlH_4$ is insoluble in 1,3,5-trimethylbenzene and is a weak reducing agent in aromatic solvents.[34] Consequently, reduction of $NiCl_2$ proceeds only slightly in refluxing 1,3,5-trimethylbenzene (eqs 1 and 2), while $LiAlH_4$ thermally decomposes to LiH and metallic Al.[35] The $NiCl_2$, $NiCl_x$ ($x < 2$), LiH, and nano-Al then react when the solid residues from the solvent step are heated to higher temperatures (290−350 °C), generating nano-Ni. Thus, nano-Ni and nano-Al form as separate phases. Subsequently or simultaneously the nano-Al and nano-Ni combine exothermically to produce nickel aluminides.

The highly exothermic reactions of Ni and Al powders to generate nickel aluminides have been extensively investigated.[36−38] Such processes are referred to variously as self-propagating high-temperature syntheses (SHS), thermal explosions (TE), or reactive-sintering (RS) procedures.[39−41] The distinguishing characteristic of SHS/TE/RS processes is that once initiated the reaction exothermicity provides the thermal activation, such that they proceed rapidly, spontaneously, and generally at high achieved temperatures. The temperature jumps and expulsion of powder and pellet fragments from the furnace during annealing of the as-deposited products of eqs 1 and 2, and mixtures of nano-Ni and nano-Al indicate that these processes belong to the SHS/TE/RS class.

The exothermic reactions of the as-deposited powders from eqs 1 and 2 also resemble the solid-state metathesis (SSM) processes described by Kaner.[42−44] In SSM reactions, the generation of byproduct alkali-metal halide salts (such as LiCl) provides the large thermodynamic driving force for the rapid, spontaneous, high-temperature process.[42−44] In traditional SHS/TE/RS processes the heat of formation of the desired product alone provides the thermodynamic driving force, and no byproducts are produced.[3,40] In our cases from eqs 1 and 2, both byproduct salts and intermetallic compounds are produced, and both contribute to the driving force for the reaction.

SHS/TE/RS processes normally initiate (ignite) when a portion of the sample is heated to temperatures near the lowest eutectic temperature (640 °C in the Ni−Al system).[36,43] The formation of a liquid phase provides large interfacial contact areas and allows facile reactant diffusion, generally promoting completion of the reaction within a few seconds.[41] The ignition temperatures of 300−400 °C we observed are ≥200 °C lower than those observed in coarse-grained mixtures of Ni and Al,[36] suggesting that intimate mixing of reactants on the nanometer scale facilitates interfacial reaction and local heating to near the eutectic temperature.

SHS/TE/RS processes are not generally known to produce nanocrystalline products, because reactant

(34) Seyden-Penne, J. *Reductions by the Alumino- and Borohydrides in Organic Synthesis*; VCH: New York, 1991; p 3.
(35) Wiberg, E.; Amberger, E. *Hydrides of the Elements of Main Groups I-IV*; Elsevier: New York, 1971; p 416.
(36) Stoloff, N. S.; Alman, D. E. *Mater. Sci. Eng., A* **1991**, *144*, 51−62.
(37) Williams, W. C.; Stangle, G. C. *J. Mater. Res.* **1995**, *10*, 1736−1745.
(38) Niedzialek, S. E.; Stangle, G. C.; Kaieda, Y. *J. Mater. Res.* **1993**, *8*, 2026−2034.
(39) Cahn, R. W. *Adv. Mater.* **1990**, *2*, 314−316.
(40) Yi, H. C.; Moore, J. J. *J. Mater. Sci.* **1990**, *25*, 1159−1168.
(41) Zhang, Y.; Stangle, G. C. *J. Mater. Res.* **1994**, *9*, 2592−2604.
(42) Wiley: J. B.; Kaner, R. B. *Science* **1992**, *255*, 1093−1097.
(43) Gillan, E. G.; Kaner, R. B. *Chem Mater.* **1996**, *8*, 333−343.
(44) Treece, R. E.; Gillan, E. G.; Kaner, R. B. *Comments Inorg. Chem.* **1995**, *16*, 313−337.

particle sizes are usually large, and intermediate liquid phases typically support extensive grain growth.[39−41] Retention of nanometer-scale grain sizes in the present cases likely results from the presence of byproduct salt or reinforcement (AlN) diluents in most of them, which limit the maximum reaction temperatures achieved, and the porous, low-density reactant microstructures, in which grain growth is suppressed. Kaner and Wiley have previously discussed suppression of grain growth by an NaCl diluent phase in conjunction with the SSM synthesis of nanocrystalline MoS_2.[42] If the product intermetallics had precipitated from a continuous, extensive liquid phase in our cases, larger crystallite sizes and coarser microstructures should have resulted. Grain growth is presumably also limited by the short duration of the high-temperature excursions.

As noted above, all of our consolidated nickel aluminide samples were significantly oxidized (containing 8−19 wt % O). Although nanocrystalline aluminum and aluminide intermetallics are inherently prone to adventitious oxidation, it is exacerbated by the porous microstructures that nanocrystalline powders typically possess. We previously reported that despite the high oxygen sensitivity of nano-Al, samples could be chemically synthesized that contained only 0.25 wt % O.[18] In that case, because of the low crystallization temperature of Al,[45,46] nanocrystallites grew at low temperatures and precipitated from solution as tight aggregates in which most nanocrystallite surfaces were protected from adventitious oxidation.[18] However, in the present cases the nickel aluminides form initially as amorphous phases or porous agglomerates that expose large surface areas, and hence are readily adventitiously oxidized. The high melting temperatures of NiAl and Ni_3Al likely preclude nanocrystallization and aggregation during the solution-phase step.[18,45,46] Impurity contamination due to high environmental sensitivity is a problem common to many nanocrystalline *powders*.[18] Thus, alternative procedures for fabricating consolidated nanocrystalline materials should be pursued that avoid powders and exposure of large nanocrystallite surface areas, such as by devitrification of metallic glass[47] or severe plastic deformation.[11]

To our knowledge, single-component nanocrystalline nickel aluminide specimens having good tensile properties and exhibiting superplasticity have been reported in only one study.[8] In that study, the nanocrystalline nickel aluminides were fabricated by severe plastic deformation,[8] which does not involve nanocrystalline *powders*, and consequently does not suffer the adventitious oxidation encountered here. Manipulation of nanocrystalline nickel aluminide powders will not be readily experimentally achievable, because of their extremely high oxygen sensitivities.[18,28] Gas condensation,[9] mechanical attrition,[10] and chemical synthesis all generate intermediate nanocrystalline powders, and are therefore unsuitable for fabricating single-component (pure) nanocrystalline nickel aluminides.

In summary, nanocrystalline nickel aluminide powders are inherently susceptible to adventitious oxidation. All of the consolidates generated via eqs 1−4 were nanocomposites containing alumina, and not single-component nickel aluminides. Consequently, we did not evaluate the tensile strength or superplasticity of these materials. The consolidates produced from admixtures of nano-Ni and nano-Al powders possessed the lowest oxygen levels and good environmental stability. Those containing AlN nanowhiskers exhibited the highest Vickers microhardnesses.

Experimental Section

General Procedures and Materials. All ambient-pressure procedures were carried out under dry N_2 or Ar using standard inert-atmosphere techniques. $NiCl_2$ (98%) and $LiBEt_3H$ (1.0 M in THF) were purchased from Aldrich and used without further purification. $LiAlH_4$ (95% purity, Aldrich), was typically used without further purification for reactions conducted in 1,3,5-trimethylbenzene. For reactions conducted in Et_2O the insoluble gray impurities were removed from the $LiAlH_4$ by filtering the Et_2O solution, which was then either used directly, or the Et_2O was removed in vacuo to yield a purer, white, $LiAlH_4$ solid. No significant differences in the products from purified and unpurified $LiAlH_4$ were detected. Nano-Al[27] and nano-AlN[28,29] were prepared by literature procedures.

Diethyl ether (Et_2O) and hexane (with a few drops of added tetraethylene glycol dimethyl ether) were distilled from sodium benzophenone ketyl and stored over type 4A sieves. 1,3,5-Trimethylbenzene (97%, Aldrich) was washed in a separatory funnel with concentrated H_2SO_4 until colorless, and then washed successively with deionized H_2O, 5% NaOH, and deionized H_2O. The 1,3,5-trimethylbenzene was then predried over CaH_2, distilled from sodium/potassium benzophenone ketyl and stored over type 4A sieves. Pyridine (99.99%, Fisher) was refluxed over KOH for 4 days, distilled, and stored over type 4A sieves. MeOH was refluxed over magnesium turnings activated with iodine, distilled, and stored over type 3A sieves.

Procedures for X-ray diffraction (XRD),[48] electron-microprobe analyses,[49] transmission electron microscopy (TEM), scanning electron microscopy (SEM), energy dispersive spectroscopy (EDS), solid-state NMR, Vickers microhardness determination, and pellet consolidation are given in the Supporting Information.

Elemental Analyses. Two samples of powder generated by eq 1 were subjected to combustion analyses, conducted by Oneida Research Services in Whitesboro, NY. The first sample was as-precipitated powder from eq 1 and dried in vacuo at room temperature, which gave (element, wt %) C, 1.13; H, 0.39; Cl, 35.9; N, 0.00. The second sample was powder precipitated from eq 1 and dried in vacuo at 100 °C for 5 h, which gave C, 0.97; H, 0.29; Cl, 36.9; N, 0.00. These values were used in conjunction with the solid-state NMR studies; see the Results section.

Preparation of Nano-Ni. $LiBEt_3H$ (0.54 mol) as a THF solution was added to a slurry of $NiCl_2$ (26.78 g, 0.21 mol) in 1,3,5-trimethylbenzene (300 mL) at room temperature. No evidence of reaction was visually apparent at this stage. The THF was removed in vacuo, and the remaining slurry was refluxed for 20 h. The resulting black powder (43.7 g) was collected on a glass frit, and successively washed with 130 mL of hexane, 250 mL of MeOH (0 °C), and 4 × 50 mL of N_2-sparged, HPLC-grade H_2O. The remaining solid was dried in vacuo to yield nano-Ni as a fine black powder (12.6 g, 102% yield), which was characterized by XRD, TEM, and EDS as described in the Results section.

Preparation of NiAl in Et_2O (Eq 3). A solution of $LiAlH_4$ (7.14 g, 0.188 mol) in Et_2O (150 mL) was chilled to −20 °C and added dropwise to a stirred slurry of $NiCl_2$ (15.59 g, 0.120 mol) in Et_2O (80 mL) at −20 °C. The orange $NiCl_2$ slurry

(45) Gleiter, H. *Prog. Mater. Sci.* **1989**, *33*, 223−315.
(46) Birringer, R. *Mater. Sci. Eng., A* **1989**, *A117*, 33−43.
(47) Zhong, Z. C.; Jiang, X. Y.; Greer, A. L. *Phil. Mag. B* **1997**, *76*, 505−510.
(48) Hellstern, E.; Fecht, H. J.; Fu, Z.; Johnson, W. L. *J. Appl. Phys.* **1989**, *65*, 305−310.
(49) Armstrong, J. T. *Microbeam Anal.* **1988**, 239−246.

turned black upon addition of the first drops of $LiAlH_4$. The black slurry was maintained at ca. −20 °C throughout the addition of $LiAlH_4$ and then stirred at room temperature for 16 h. The resulting black solid (26.32 g) was collected and dried in vacuo.

A 16.47 g portion of the as-precipitated black solid was loaded into a fused-silica tube (45 cm × 2.5 cm) sealed at one end with an 8 mm diameter constriction in the middle. The tube was connected to a vacuum line via a valve and vacuum tubing and was inserted into a tube furnace so that the constriction was just outside. The tube and contents were annealed under a dynamic vacuum of 10^{-3} Torr (10^{-1} Pa) at 650 °C for 40 h and then at 750 °C for 40 h. White LiCl and a colorless to pale-yellow liquid collected in the tube outside the furnace. The tube was allowed to cool and was then transferred to a N_2-filled glovebox. The tube was then broken at the constriction to separate the byproducts and the $NiAl/Al_2O_3$ product (7.04 g, 87% yield) was recovered from the bottom of the tube. The $NiAl/Al_2O_3$ powder was characterized as described in the Results section.

Preparation of Ni_3Al in Et_2O (Eq 4). The procedure for the preceding preparation (NiAl in Et_2O) was repeated here, using the following quantities: $LiAlH_4$ (4.87 g, 0.128 mol) in Et_2O (80 mL), and $NiCl_2$ (17.80 g, 0.137 mol) in Et_2O (100 mL). A black solid (21.50 g) formed, a portion (20.73 g) of which was annealed as above at 650 °C for 10 h and then at 750 °C for 40 h. The resulting Ni_3Al/Al_2O_3 product (9.00 g, 85% yield) was characterized as described in the Results section.

Preparation of NiAl in 1,3,5-Trimethylbenzene (Eq 1). A slurry of $NiCl_2$ (10.56 g, 81.5 mmol) and $LiAlH_4$ (3.98 g, 105 mmol) in 1,3,5-trimethylbenzene (120 mL) was refluxed for 16 h. The resulting tan-gray powder (13.62 g) was collected and annealed using the procedure described above (for NiAl in Et_2O) under 10^{-3} Torr (10^{-1} Pa) at room temperature for 20 h, at 150 °C for 7 h, at 550 °C for 18 h, and then at 650 °C for 2.5 h. The NiAl product (4.47 g, 64.0% yield) was recovered and characterized as described in the Results section.

Caution! During the annealing process as the powder sample was heated to 550 °C a sudden reaction occurred that generated a large volume of H_2 gas (see the Results section). In several instances sealed annealing tubes and even tubes under dynamic vacuum burst and were propelled from the furnace. Therefore, the tubes in which the powders are heated must have sufficiently large volumes to safely accommodate the sudden gas evolution.

Preparation of Ni_3Al in 1,3,5-Trimethylbenzene (Eq 2). The procedure for the preceding preparation (NiAl in 1,3,5-trimethylbenzene) was repeated here using the following quantities: $NiCl_2$ (15.55 g, 120 mmol), $LiAlH_4$ (3.44 g, 90.6 mmol), and 1,3,5-trimethylbenzene (120 mL). The resulting powder (22.46 g) was annealed in vacuo according to the schedule in the preceding preparation. The Ni_3Al product (4.47 g, 55% yield) was recovered and characterized as described in the Results section.

Large-Scale Annealing Procedure. The large quantities (>12 g) of as-precipitated powder from eqs 1 or 2 required to provide sufficient material for consolidation were annealed in 7 cm diameter, 45 cm length, fused-silica tubes constricted to 2.5 cm in the middle and to a 2.5 cm tube on the open end. In each such case, powder was loaded into a tube in an N_2-filled glovebox, and the tube was closed with a Cajon-Ultratorr fitting-and-valve assembly, which was wired in place. The tube was then connected to a vacuum line, placed in a tube furnace, and annealed as described above. Upon initiation of the sudden, exothermic reaction near 400 °C, such tubes were observed to visibly recoil.

Preparation of Ni_xAl_y and Ni_xAl_y/AlN Nanocomposites from Nanocrystalline Admixtures. Nano-Al (mean particle diameter 50−130 nm),[27] nano-Ni (mean particle diameter 8 nm), and nanowhisker-rich nano-AlN (mean whisker diameter 44−50 nm)[28,29] were combined in the appropriate ratio for the desired intermetallic phase (NiAl or Ni_3Al) and amount of ceramic reinforcement. The combined powders were then cosuspended in pyridine or hexane by sonication in a cleaning bath for 1.5−3.5 h to thoroughly admix them. The suspending liquid was removed in vacuo while sonication continued to prevent selective agglomeration and resegregation of the nanoparticles by composition. The resulting intimately mixed powders were consolidated into pellets by pressing at 350 MPa for 0.75 to 3.0 h at room temperature, and then at 350 MPa for 0.75 to 1.0 h at 1000−1200 °C to effect reaction. The compositions of the powder mixtures and conditions for suspension and consolidation of the powders are given in Table 2.

Acknowledgment. This work was funded by NSF grants CHE-9158369 and CHE-9709104 to W.E.B., and NSF grant DMR-9705080 to M.S.C. J.A.H. was partially supported by a Department of Education GAANN grant (P200A40147). The authors thank D. T. Kremser for microprobe analyses, and D. L. Rempel, C. Frederickson, and R. Criss for mass-spectrometric analyses. J.A.H. thanks P. C. Gibbons and K. F. Kelton for helpful discussions.

Supporting Information Available: Figures S1−S10 and additional experimental details (PDF). This material is available free of charge via the Internet at http:///pubs.acs.org.

CM9905186